J Mater Sci (2009) 44:1456–1461
DOI 10.1007/s10853-008-3036-9

Microstructure–properties relationship in ceramic–elastomer composites with 3D connectivity of phases

Kamil Babski · Anna Boczkowska · Krzysztof J. Kurzydlowski

Received: 27 February 2008 / Accepted: 7 October 2008 / Published online: 6 November 2008

Abstract The ceramic–elastomer composites with 3D phase connectivity were tested under compressive loads. Such composites exhibit high initial strength and stiffness with the ability to sustain large deformations. Samples of the composites were made of porous SiO_2 ceramic matrix infiltrated by polyurethane elastomer. The ceramic matrix preforms used differed in the porosity and three different composite microstructures have been obtained. Selected parameters of microstructure composites were evaluated using image analysis. The compressive strength and capacity for energy absorption are characterized under various strain rates (0.001–235 s^{-1}). It was found that stress–strain characteristic depends on the strain rate and the specific interface area (Sv). Pore size and the specific interface area have a strong effect on the compressive strength of composites and these parameters can be used for tailoring their mechanical properties. The acoustic emission was applied to identify stages in the process of microstructure damage during compression. The interpretation of damage stages was proposed, which also explains the character of the stress–strain curves.

K. Babski (✉) · A. Boczkowska · K. J. Kurzydlowski
Faculty of Materiale Science and Engineering, Warsaw University of Technology, Woloska 141, Warsaw 02-507, Poland
e-mail: kbabski@inmat.pw.edu.pl

A. Boczkowska
e-mail: abocz@mail.pw.edu.pl

K. J. Kurzydlowski
e-mail: kjk@inmat.pw.edu.pl

Introduction

The ceramic–elastomer composites can be obtained via infiltration of porous ceramic preform by urethane elastomer. Such composites exhibit 3D connectivity of phases and can offer some new properties when compared to common, ceramic particle-reinforced polymers. The infiltration of porous matrix with elastomer provides a significant increase in the mechanical properties. This can be an advantage in many commercial applications, now limited by the poor mechanical properties of porous ceramics, which include impact or damage tolerant elements or bone grafts [1–3].

Ceramic–elastomer composites exhibit higher initial compressive strength in comparison to porous ceramics and sustain larger deformations. The stress plateau over a wide strain level is observed on the stress–strain compressive curves. Although during compression the composite microcracking occurs, the composites maintain cohesion and are able to dissipate mechanical energy.

Ceramic–elastomer composites combine the initial stiffness of ceramics, rubbery elasticity and damping properties of elastomer. Such composites absorb energy more efficiently than both components separately. The energy absorbance capacity and properties under compression are comparable to some aluminium foams and energy-absorbing composite structures [4–10]. Such materials can be used as a part of lightweight shielding or panels for protecting objects and structures against impact loads.

In this work, the mechanical properties and energy absorption of the composites were estimated in compression at quasistatic and dynamic strain rate conditions.

Materials and methods

Porous SiO_2 preforms were used for infiltration, as the potential applications of composites require relatively low-cost materials and processing. The preforms were obtained from the SiO_2 powders with controlled particle size. In applied method, the open porosity forms from voids present between particles of powders. Ceramic powders were mixed with 5% of a low-temperature glass binder, pressed and sintered in air at 950 °C [11]. The studies were conducted on samples with similar porosity but three different pores sizes. The size fraction of applied powders, obtained pore size and porosity of the sintered ceramics are presented in Table 1.

The sintered porous preforms were infiltrated with urea-urethane elastomer at elevated temperature (approximately 100 °C) in vacuum, in order to evacuate air and force the liquid to penetrate the network of pores. As evaluated previously [11], such conditions assume proper infiltration with over 98% of open pores fully filled with elastomer.

The urea–urethane elastomer for infiltration was obtained from oligoethyleneadipate, diisocyanate and dicyandiamide. Such composition of substrates forms a liquid mixture with relatively low initial viscosity, desired for infiltration process of a structure with fine pores. The extensive characterization of urea-urethane elastomer can be found in [12].

The quantitative characterization of the microstructure was carried out on plane sections of composites using image analysis methods [13]. A commercial software Micrometer was used. The parameters determined were: Vv—the volume fraction of elastomer and Sv—the specific area of interphase boundaries (surface area in unit volume).

The composites were subjected to quasistatic (0.001 s^{-1}, 2 s^{-1}) and dynamic (235 s^{-1}) compressive loads to determine their energy absorption characteristic and strength–strain rate dependence. It is assumed that the strain rates range employed here is typical of automobile crash accidents [10]. Samples were tested between parallel steel plates. The sample edges were precisely machined to assure parallel orientation for proper loading conditions. For quasistatic loading, the MTS 810 testing machine was used. The strain of samples was estimated based on the machine traverse displacements. True traverse speed was 0.017 and 40 mm/s. For impact loading, a drop hammer Instron Dynatup 9250HV was used. The mass and height of the impact hammer were adjusted for a 100 N impact energy and the initial speed of impact hammer was 4.7 m/s. The velocity and the displacements were obtained by integrating the acceleration with respect to time. The drop mass test does not allow a constant velocity of the ram during the compression stroke. For this reason, the quasistatic and dynamic results may not be directly comparable. However, the deceleration of the ram in the early stage of straining the sample may not drastically affects the results.

Table 1 Characteristics of the porous ceramics used in this study

Type	Particle size of the ceramic powder (μm)	Mean pore size (water bubble method) (μm)	Open porosity (Archimedes method) (%)
A	<63	20	43 ± 2
B	200–300	70	41 ± 2
C	500–1000	120	39 ± 2

Results and discussion

Image analysis

The observations of the microstructure were performed using a scanning electron microscope Hitachi 3500S in a low-vacuum mode. Images of plane sections of three types of samples are presented in Fig. 1.

The results of image analyses are listed in Table 2.

Stress–strain characteristics under compressive loads

The representative stress–strain curves obtained in compression tests for porous ceramic, elastomer and composite are presented in Fig. 2.

The elastomer itself exhibits high elasticity and reversible strains. The porous ceramic fractures rapidly after reaching a critical stress level. The composite compressive strength is much higher than the strength of ceramic. Moreover, what is remarkable is that, when the ceramic structure starts to collapse rapidly, a large stress plateau is observed and composites can still transmit significant force and sustain large deformations. After unloading, composite samples tend to return to their initial shape and lose the initial stiffness. However, they are still able to transmit forces when re-loaded.

Since the stress–strain curve for composites has a non-linear characteristic, some loading stages can be identified during their straining. These stages are related to the type and localization of microstructure damage [14–16] as was identified by the acoustic emission [17] (Fig. 3).

The first stage "I" is an elastic region, where the stresses arise with no acoustic signal from the sample. The second stage "II" can be identified as a stable nonlocalized microcracking [14]. In this stage, some microcracking occurs in various positions within the entire gauge volume of the sample which can still sustain increasing stresses. The next stage "III" features localization of microcracking. The cracks start to grow along in parts of the composite and the

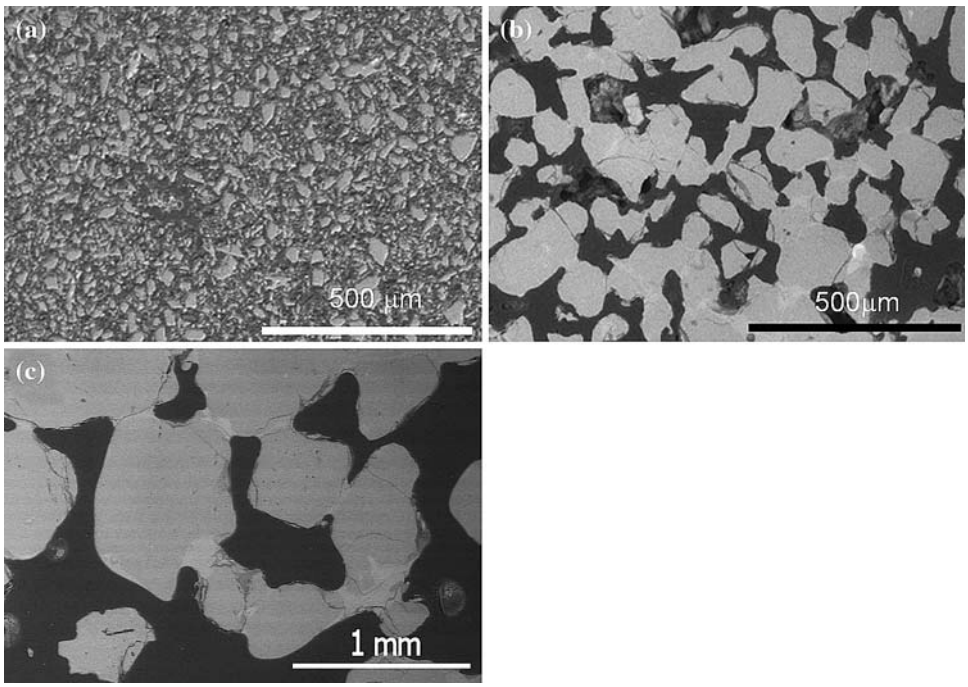

Fig. 1 SEM images of plane sections of "A", "B" and "C" types of ceramic–elastomer composite

Table 2 Microstructure parameters of porous ceramic obtained from image analysis

Composite type	Mean particle size of ceramic powder (μm)	Vv (volume fraction of elastomer)	Sv (specific area of phase boundary) (1/mm)
A	<63	0.41 ± 0.04	64.5 ± 3.8
B	200–300	0.37 ± 0.02	14.2 ± 1.3
C	500–1000	0.38 ± 0.03	4.6 ± 0.7

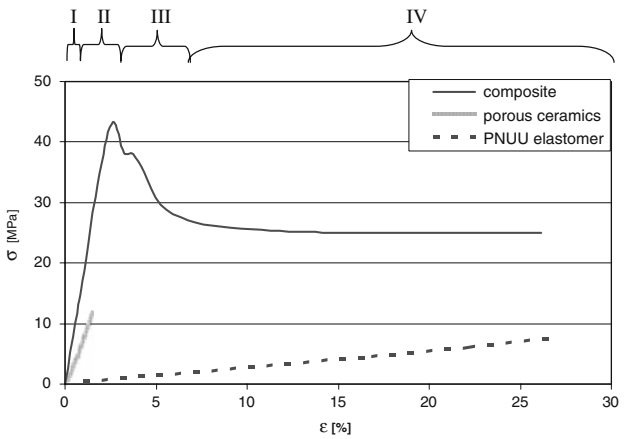

Fig. 2 Representative compressive stress–strain curves of porous ceramic, elastomer and ceramic–elastomer composites

ceramic skeleton starts to collapse. From that point there is no more increase in transmitted stresses. In the last stage, unstable microcracking occurs with the structure collapsing rapidly and a significant drop of stresses. The above-described stages can overlap and the borders between them are "diffuse".

It was revealed that over 98% of open pores in the ceramic preforms are fully filed with an elastomer. Since the open porosity and the Vv parameter for all types of composites are similar (within the tolerance interval), the Sv parameter varied significantly from value 4.6 for "C" up to 64.5 for "A" type microstructure. It is expected that the specific area of interface boundary (Sv) might impact the mechanical properties of the composite.

Microstructure–properties relationship and strain rate dependence

Typical stress–strain response for the three types of composites at different strain rates are presented in Fig. 4. All curves show typical behaviours, as discussed in the further text.

The properties of composites were estimated from the stress–strain curves for both quasistatic and dynamic tests. Since during dynamic tests, the strain rate is not constant, the curves were analysed only up to 25% of strain. For this value of strain the hammer decelerates by about 50%.

In Fig. 5, the strain rate effect on the maximum compressive stress is presented in semi-logarithmic scale.

The maximum compressive strength depends on the composite microstructure and also on applied strain rate. The response of the composite samples to straining rate is not linear. As the straining rate increases, critical amount of defects in ceramic matrix are achieved faster. Also, the

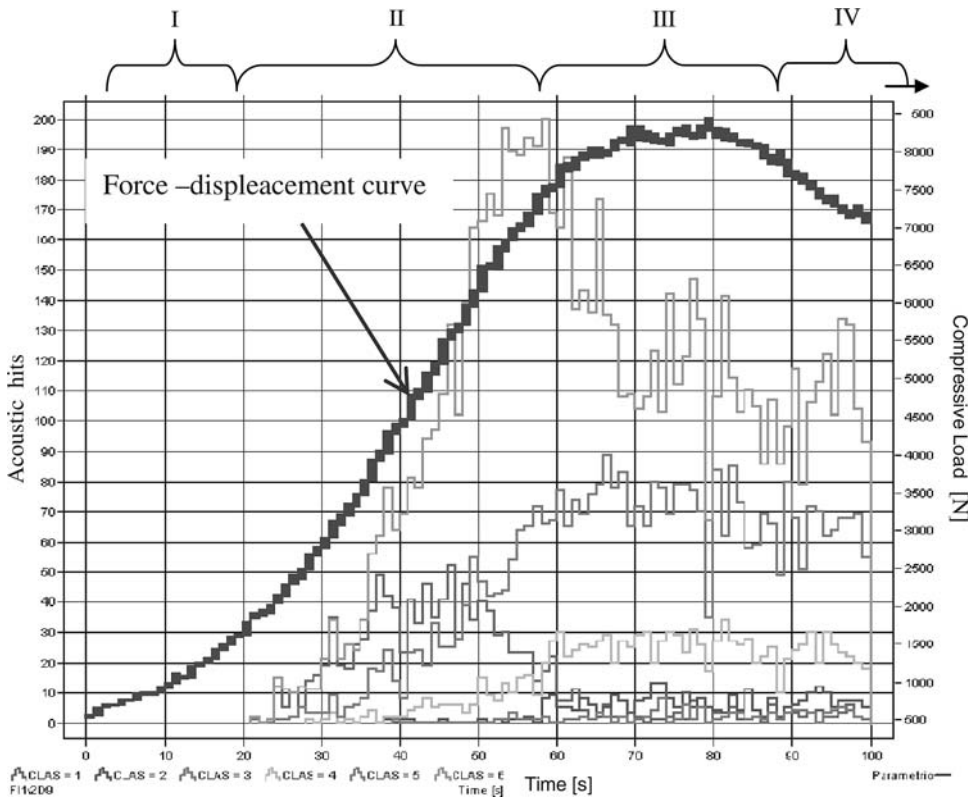

Fig. 3 Acoustic emission signal during compressing of composite sample

elastomer modulus is strain rate dependent. The composite type "A" is the most sensitive to strain rate with the highest Sv value. This can be due to the fact that for high Sv value the elastomer within the microstructure is highly constrained and high strain gradients occur in it. High strain gradients and high interface area between the ceramic and elastomer increase the maximum compressive stress transmitted in the composites with percolated structure.

The effect of the relative interface area (Sv) on maximum compressive stress is presented in Fig. 6.

The differences in the maximum compressive strength for composites loaded with the same straining rate are affected mainly by differences in the initial compressive strength of porous ceramic. The composite type "A", made of ceramic with the finest grains and pores, has the highest compressive strength. This might be because of the fine porous structure, which has a higher density of ceramic necks per unit volume. As a result, the critical accumulation of defect occurs at higher stresses. For the same processing conditions of porous ceramic, small particles tend to sinter better and as a result the probability of defects formation is lower. Regarding the sample size, stresses in fine microstructure may be distributed more uniformly. As it is shown in Fig. 6, the dependence between Sv and maximum compressive stress is logarithmic.

As expected, the absorbed energy increases for high strain rates. This effect is primarily caused by the viscoelastic properties of the elastomer, and to a less degree by the microstructure of the ceramic skeleton. Since strain energy is stored in the elastomeric components as well, samples were loaded and unloaded in order to estimate the dissipated energy.

For the investigated composites and the strain rates employed, the relationship between the absorbed energy and the strain rate can be approximated by a logarithmic function (Fig. 7). Beyond a certain level of the strain rate, the absorbed energy for composite type "A" and "B" is similar. The correlation of the microstructure parameter Sv with energy is revealed in Fig. 8.

This suggests that there is an upper limit of the energy that can be absorbed by the composite with a given value of Sv. In other words, the absorbed energy depends on the strain rate up to a certain level, which is correlated with the value of Sv parameter.

Conclusions

It has been shown in this study that infiltration with elastomer significantly increases compressive strength of porous ceramics and prevents from rapid decohesion. By combining the porous ceramics and elastomer, one can obtain composites that effectively absorb the energy in the way comparable to some aluminium foams or energy-absorbing structures.

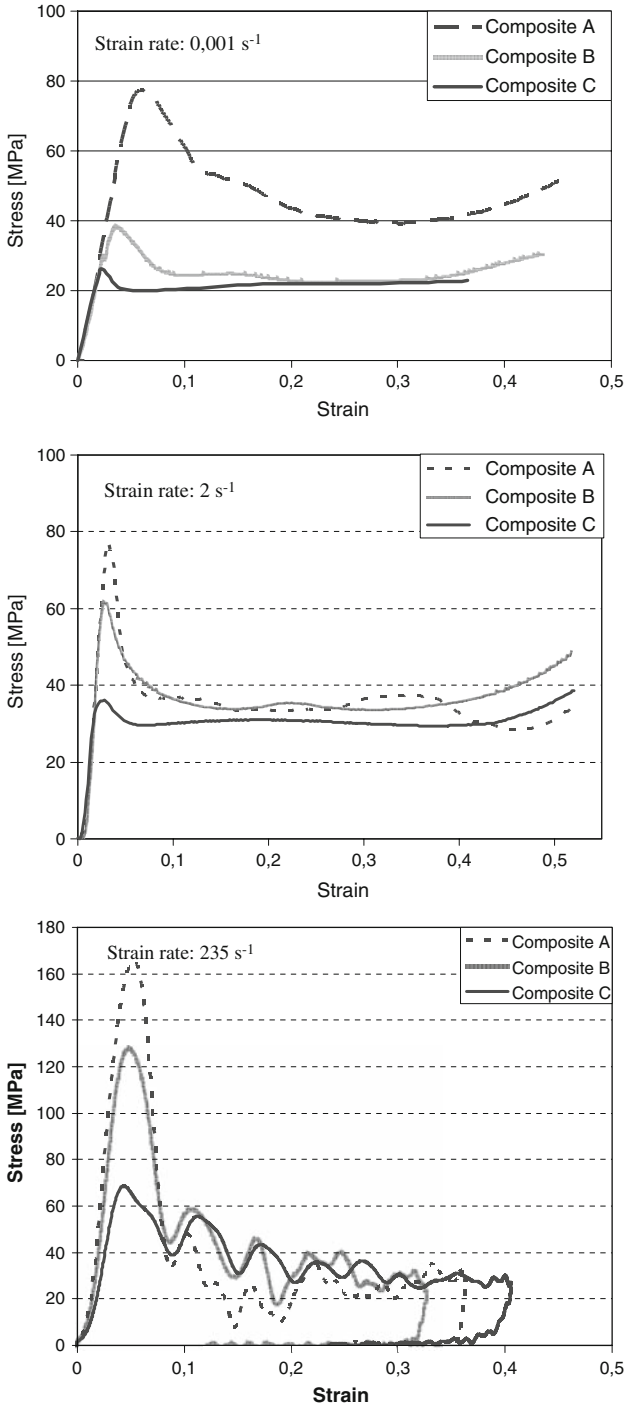

Fig. 4 Typical stress–strain curves for the composites loaded at different strain rates (0.001 s^{-1}, 2 s^{-1}, 235 s^{-1})

Since the investigated composites have a nonlinear characteristic during compression, distinct loading stages can be identified during their straining. The acoustic emission helps to identify these stages on the stress–strain curves.

The compression tests reveal a significant difference in the maximum compressive strength and absorbed energy depending on the composite microstructure and straining

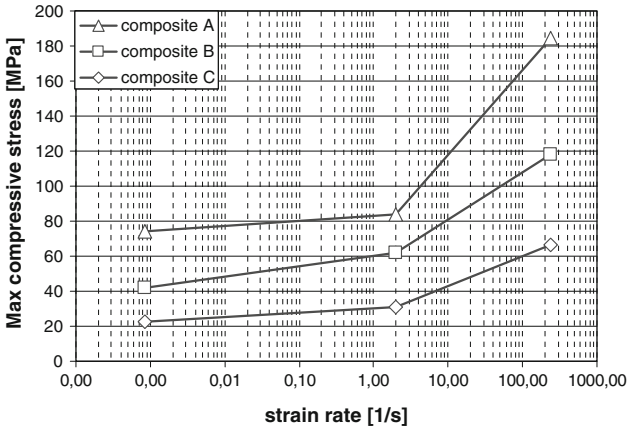

Fig. 5 The relationship between maximum compressive stresses and strain rate for different composites

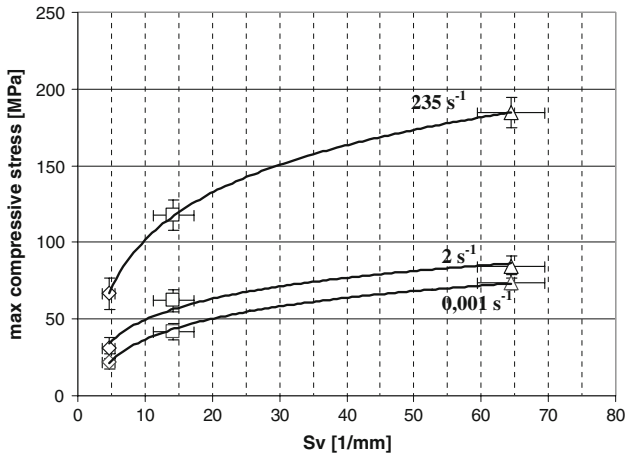

Fig. 6 The relationship between Sv and maximum compressive stress for different straining rates

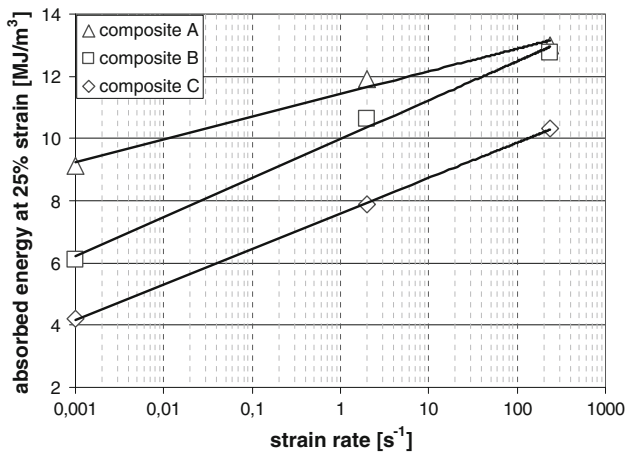

Fig. 7 The relationship between the absorbed energy and the strain rate

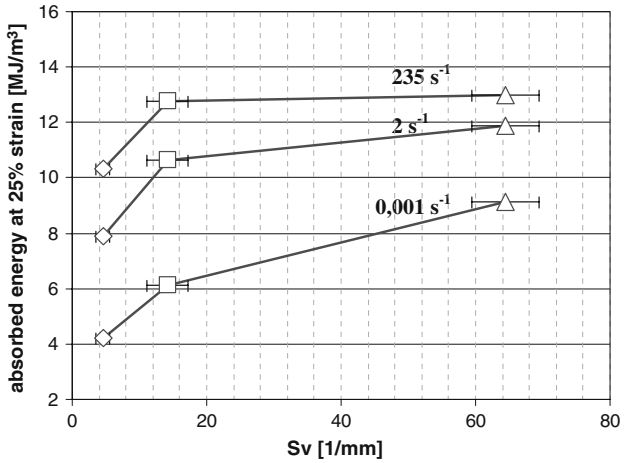

Fig. 8 The relationship between the absorbed energy and Sv parameter

rate. It was found that the maximum compressive stress in compression correlates with the specific interface area (Sv) following a logarithmic dependence. Composite type "A" (Sv = 65.5) exhibits about 300% higher maximum compressive strength than composite type "C" (Sv = 4.6) at a given strain rate.

For the investigated composites and applied strain rates, the relationship between the absorbed energy and the strain rate can be approximated by logarithmic function. At high strain rates, the relative interface area does not affect the amount of absorbed energy.

It has been shown in this study that infiltrated porous ceramic–elastomer composites are a potential energy-absorbing material with the possibility of tailoring their microstructure and properties.

Acknowledgements Authors are thankful to Prof. Mikołaj Szafran from Warsaw University of Technology, Faculty of Chemistry for processing the porous SiO_2 ceramics, Dr. Jerzy Schmidt from Krakow University of Technology for acoustic emission experiments, and Dr. Dariusz Rudnik and Piotr Lasota from Motor Transport Institute in Warsaw for providing access to the Instron Dynatup testing machine. This work was supported by Polish State Committee for Scientific Research, grant no. 3T08E 009 28.

References

1. Chen Y-C, Wu S (2004) Ceram Int 30:69
2. Cui C, Baugmann RH, Iqbal Z, Dahlstrom DK (1997) Synth Mater 85:1391
3. Kalita SJ, Bose S, Hosick HL, Bandyopadhyay A (2003) Mater Sci Eng C 23:611
4. Koza E, Leonowicz M, Wojciechowski S, Simancik F (2003) Mater Lett 58:132
5. Yang IY, Lee KS, Park SG, Cha CS (2007) J Mater Process Technol 187–188:136
6. Xue P, Yu TX, Tao XM (2000) Composites Part A 31:861
7. Mahadi E, Hamouda AMS, Sahari BB, Khalid YA (2003) Appl Compos Mater 10:67
8. Woldesenbet E, Gupta N, Jadhav A (2005) J Mater Sci 40:4009. doi:10.1007/s10853-005-1910-2
9. Gupta N (2007) Mater Lett 61:979
10. Lee DG, Lim TS, Cheon SS (2000) Compos Struct 50:381
11. Boczkowska A, Babski K, Konopka K, Kurzydłowski KJ (2006) Mater Charact 56:389
12. Konopka K, Boczkowska A, Batorski K, Szafran M, Kurzydłowski KJ (2004) Mater Lett 58:3857
13. Kurzydlowski KJ, Ralph B (1995) Quantitative description of microstructure of materials. CRC Press, Boca Raton
14. Podrezov YM, Firstov SO, Szafran M, Kurzydłowski KJ (2003) E-MRS Fall Meeting 2003 Conference, Poland
15. Wang EZ, Shrive NG (1995) Eng Fract Mech 52(6):1107
16. Blechman I (1997) Int J Solids Struct 34(20):2536
17. Boczkowska A, Konopka K, Schmidt J, Kurzydłowski KJ (2004) Composites 4(9):41